Struct Multidisc Optim (2017) 55:257–277
DOI 10.1007/s00158-016-1495-1

RESEARCH PAPER

An evaluation of constraint aggregation strategies for wing box mass minimization

Andrew B. Lambe[1] · **Graeme J. Kennedy**[2] · **Joaquim R. R. A. Martins**[3]

Received: 1 February 2016 / Revised: 12 May 2016 / Accepted: 23 May 2016 / Published online: 4 June 2016

Abstract Constraint aggregation makes it feasible to solve large-scale stress-constrained mass minimization problems efficiently using gradient-based optimization where the gradients are computed using adjoint methods. However, it is not always clear which constraint aggregation method is more effective, and which values to use for the aggregation parameters. In this work, the accuracy and efficiency of several aggregation methods are compared for an aircraft wing design problem. The effect of the type of aggregation function, the number of constraints, and the value of the aggregation parameter are studied. Recommendations are provided for selecting a constraint aggregation scheme that balances computational effort with the accuracy of the computed optimal design. Using the recommended aggregation method and associated parameters, a mass of within 0.5 % of the true optimal design was obtained.

Keywords Structural optimization · Constraint aggregation · Stress constraints · Kreisselmeier–Steinhauser function · Induced aggregation

✉ Andrew B. Lambe
alambe@yorku.ca

[1] Department of Mechanical Engineering, York University Toronto, Ontario, Canada

[2] School of Aerospace Engineering, Georgia Institute of Technology Atlanta, Georgia, USA

[3] Department of Aerospace Engineering, University of Michigan Ann Arbor, Michigan, USA

1 Introduction

We are interested in the problem of minimizing structural mass subject to constraints on structural failure. In particular, we are interested in failure criteria based on yield stress and buckling under static loads. Checking the failure criteria in the optimization problem is desirable from an engineering design perspective because doing so allows us to immediately verify that the structure is suitable for the prescribed loading conditions.

The primary issue with including failure constraints directly in the structural optimization problem is the resulting size of the optimization problem. Conceptually, for a continuum structure, failure constraints need to be enforced throughout the material domain, leading to an infinite number of constraints. More practically, failure constraints may be enforced element-wise in the finite element model. For detailed, high-fidelity structural models, this can lead to an optimization problem with many thousands or millions of failure constraints. These constraints are costly to enforce because they can only be checked by completing the structural analysis. Specialized algorithm implementations are required to solve the optimization problem efficiently (Duysinx and Bendsøe 1998).

The number of constraints in the optimization problem can be reduced through aggregation. The constraint aggregate then represents an effective failure criteria evaluated over a large part of the material domain. A natural choice for these constraint aggregates is a maximum- or minimum-value function. However, the maximum- and minimum-value functions are not differentiable and cannot be used efficiently in conjunction with gradient-based design optimization. Instead, these functions are replaced by smooth

estimators like the Kreisselmeier–Steinhauser (KS) function (Kreisselmeier and Steinhauser 1979, 1983) or the p-norm function (Duysinx and Sigmund 1998; Qiu and Li 2010). These estimators do not precisely reproduce the true feasible design space provided by the original constraints, so the final design determined by the optimizer will be different depending on the aggregation scheme.

Because of the need to aggregate failure constraints, there exists a natural compromise between the quality of the optimal structural design, i.e., how close the computed design is to the "true" optimal solution that could be computed by the model, and the computational effort to find it. This compromise has been observed in the literature before, particularly in the field of topology optimization. París et al. (2009, 2010) compared the use of local stress constraints with a global stress constraint (aggregation into one failure constraint) and block aggregation of contiguous regions of the structure. Their results confirm our intuition about the trade-off: local constraints produce the highest quality results, but block aggregation greatly reduces the computational expense. However, their results only compare a single choice for the number of blocks, or aggregation domains, with global aggregation and no aggregation. No information is given about how to choose the number of aggregation domains.

Le et al. (2010) compared aggregation based on physical location in the design domain with aggregation based on the stress distribution. In the latter scheme, an interlacing approach was used in which the elements were sorted based on the failure criteria and every m elements in order were allocated to m different constraints. While this scheme gives better control over local constraint violation, (the highly stressed elements are aggregated to many different constraints, reducing aggregation error,) it results in changes to the optimization problem formulation every time the elements are sorted and reallocated. Consequently, this changing problem statement may impede the convergence of the optimizer. Holmberg et al. (2013) study a "stress level" aggregation scheme in which elements with similar stresses are grouped in the same failure constraint. They also consider cases in which the elements are reallocated infrequently, rather than at each iteration. However, only the effects on the final solution are examined in detail in this study.

What is missing from the previous research is a detailed study of the influence of the aggregation scheme on computational effort. In this paper, we take aggregation scheme to mean both the number of constraints, the choice of aggregation function, and the choice of parameters in the aggregation function. In all cases, we take the aggregation domains to be fixed and based on physical location. While not as advanced as some of the other methods mentioned above, this approach is easy to implement, requires no *a priori* knowledge about the problem, and will not alter the problem formulation as the optimization algorithm progresses. We aim to provide general recommendations for solving failure-constrained mass minimization problems using aggregation to balance low computational effort with accuracy of the optimal solution.

Another important contribution of this work is a comparative study of classical and induced aggregation methods. Induced aggregation methods were recently introduced by Kennedy and Hicken (2015) with the aim of providing greater accuracy in the optimal solution under aggregated constraints. This paper represents the first detailed comparison of these two classes of aggregate.

Our application of interest is aircraft wing design. Our previous studies of both structural and multidisciplinary (aerostructural) wing design subject to failure constraints (Kenway et al. 2014a, b; Kennedy and Martins 2014b; Kenway and Martins 2014) generally used a small number of KS aggregation functions with a fixed choice of parameter. We have also experimented with specialized optimizers which can accommodate a large number of design constraints (Lambe and Martins 2016) and optimizers that tightly integrate adaptive constraint aggregation (Kennedy 2015). In this paper, we use a wing design problem to examine the effects of varying the aggregation scheme. Our problem contains both material yield constraints and buckling constraints.

The remainder of this paper is organized as follows. Section 2 reviews the major approaches to constraint aggregation in the literature. Section 3 lays out our wing design test problem and our analysis and optimization software. Section 4 discusses the optimization results of the different aggregation schemes. Section 5 makes recommendations for applying constraint aggregation to general mass minimization problems. Finally, Section 6 summarizes our work.

2 Review of constraint aggregation techniques

In this paper, we are concerned with minimizing structural mass subject to a bound on a measure of the local stress. We write the local stress or failure constraint as

$$g(\xi, \mathbf{x}, \mathbf{u}) \leq 1,$$

where $\xi \in \Omega$ is a point within the structural domain Ω, $\mathbf{x}$ are the design variables, and $\mathbf{u}$ are the structural degrees of freedom. Common failure constraints include the von Mises yield criterion which can be written as

$$g = \frac{\sigma_v}{\sigma_d},$$

where σ_v is the von Mises stress and σ_d is the design stress. Throughout the following, we omit the arguments to the failure function g to simplify our notation.

As previously described, one method to impose the bound $g \leq 1$ everywhere within the structural domain is to use the maximum-value function such that

$$\max_{\xi \in \Omega} g = \max g \leq 1. \tag{1}$$

However, because the constraint (1) is not smooth, efficient gradient-based optimization algorithms cannot be used to solve the resulting optimization problem. Instead, we use smooth constraint aggregation functions $\mathbf{c} \in \mathbb{R}^M$ to approximately impose $\max g \leq 1$ over M disjoint partitions of the structural domain Ω_k, $k = 1, \ldots, M$. These functions satisfy the limit property

$$\lim_{\rho \to \infty} \vec{c}_k(g, \rho) = \max_{\xi \in \Omega_k} g \qquad k = 1, \ldots, M. \tag{2}$$

Increasing the parameter ρ simultaneously reduces the aggregation error while also making the optimization problem more difficult to solve with a gradient-based optimizer due to the increased curvature in regions where the maximum-value function is not differentiable. Therefore, we are interested in selecting functions for which moderate values of ρ yield accurate constraint aggregates.

To review the different constraint aggregation approaches, we make reference to the following model problem.

$$\begin{aligned} \text{minimize} \quad & m(\mathbf{x}) \\ \text{with respect to} \quad & \mathbf{x}, \mathbf{u} \\ \text{such that} \quad & \mathbf{c}(g, \rho) \leq 1 \\ \text{governed by} \quad & \mathbf{K}(\mathbf{x})\mathbf{u} = \mathbf{f}. \end{aligned} \tag{3}$$

In this problem, $m(\mathbf{x})$ represents the structural mass, and $\mathbf{K}(\mathbf{x})\mathbf{u} = \mathbf{f}$ represents the finite element governing equations.

We solve the optimization problem (3) using two types of constraint aggregates: discrete and continuous. Discrete aggregates operate on a finite set of stress constraints that are obtained by evaluating g at trial points within the structural domain. Typically, these trial points correspond to the quadrature points in each element. As a result of this construction, some discrete aggregates exhibit mesh-dependence (Kennedy and Hicken 2015). In contrast, continuous aggregation techniques seek an approximation of the maximum value function using integrals over the domain. As a result, continuous aggregates have a well-defined limit for decreasing element size. However, for a fixed mesh the discrete and continuous aggregates share the same limit as ρ increases if the quadrature scheme for the continuous aggregate shares the same trial points as the discrete aggregate.

One elusive property of constraint aggregation methods is conservatism. An aggregate c is said to be conservative if, given a threshold parameter value ρ^*,

$$c(g, \rho) > \max g \quad \forall \rho > \rho^*. \tag{4}$$

In other words, the estimate of the maximum value produced by a conservative aggregate is necessarily an overestimate. As a result, a conservative aggregate would guarantee $g \leq 1$ everywhere within the domain. Unfortunately, to our knowledge, a truly conservative aggregate does not exist for an arbitrary stress distribution, g. While some discrete aggregates, such as the KS function and p-norm, are discretely conservative, they make no guarantees about the value of the stress constraint at points other than the trial locations (Kennedy and Hicken 2015).

2.1 Classical constraint aggregation

In this section, we review two classical approaches to constraint aggregation: Kreisselmeier–Steinhauser (KS) aggregation (Kreisselmeier and Steinhauser 1979, 1983; Akgün 2001) and p-norm aggregation (Duysinx and Sigmund 1998; Qiu and Li 2010). When applied to the continuous constraint g, these aggregation approaches reduce to functionals over the domain Ω. The KS functional is given by

$$\begin{aligned} c_{KS}(g, \rho) &= \frac{1}{\rho} \ln \left[\frac{1}{\alpha} \int_\Omega e^{\rho g} d\Omega \right] \\ &= k + \frac{1}{\rho} \ln \left[\frac{1}{\alpha} \int_\Omega e^{\rho (g-k)} d\Omega \right], \end{aligned} \tag{5}$$

where $\alpha > 0$ is a normalization factor and k is an arbitrary constant. The factor α is typically chosen to be either 1 or $|\Omega|$, but may be chosen arbitrarily provided it does not affect the asymptotic convergence of the functional at large values of ρ (Kennedy and Hicken 2015). The second form of the KS functional is preferable when using finite-precision arithmetic since very large powers of e can be avoided with a suitable choice of k. The p-norm functional is given by

$$\begin{aligned} c_{PN}(g, \rho) &= \left[\frac{1}{\alpha} \int_\Omega |g|^\rho d\Omega \right]^{\frac{1}{\rho}} \\ &= k \left[\frac{1}{\alpha} \int_\Omega \left| \frac{g}{k} \right|^\rho d\Omega \right]^{\frac{1}{\rho}} \end{aligned} \tag{6}$$

where $\alpha > 0$ and $k > 0$ have the same meaning as in the KS functional. Again, the second form of the functional is preferable when finite-precision arithmetic is used. Despite calling (6) a p-norm functional, we use ρ as the norm value for consistency in the presentation of the different methods.

The presence of the absolute value operator in the p-norm functional compromises its applicability as an aggregator. If g can take both positive and negative values, then

the functional is not differentiable in regions where g transitions from positive to negative. For some failure criteria, such as the von Mises stress criterion, this is not an issue because g is restricted to nonnegative real values. If the failure criterion has a finite, negative lower bound, such as the Tsai–Wu failure criterion, the criterion should be remapped to nonnegative real values to exploit p-norm aggregation. If g can take arbitrarily negative values, for instance in buckling envelope calculations, remapping is not possible and the KS functional is recommended instead.

Both the KS and p-norm functionals have analogues for finite sets of constraints. Let us define a finite set of constraints by selecting n_t trial points in Ω at which to check for failure. Let $\xi_i, i = 1, ..., n_t$ be the trial point locations and $g_i = g(\xi_i, \mathbf{x}, \mathbf{u})$ be the constraint values at the trial points. The KS function for this set of constraints is

$$c_{DKS}(\rho) = \frac{1}{\rho} \ln \left[\sum_{i=1}^{n_t} e^{\rho g_i} \right] = \max_i g_i + \frac{1}{\rho} \ln \left[\sum_{i=1}^{n_t} e^{\rho (g_i - \max_i g_i)} \right], \tag{7}$$

while the p-norm function is

$$c_{DPN}(\rho) = \left[\sum_{i=1}^{n_t} |g_i|^{\rho} \right]^{\frac{1}{\rho}} = \max_i |g_i| \left[\sum_{i=1}^{n_t} \left| \frac{g_i}{\max_i g_i} \right|^{\rho} \right]^{\frac{1}{\rho}}. \tag{8}$$

On the right side of both (7) and (8), we have chosen the constant k to be the maximum value of g obtained in the trial points.

2.2 Induced constraint aggregation

Recently, Kennedy and Hicken (2015) introduced a new class of aggregation methods known as induced aggregation methods. Induced aggregates are designed to provide more accurate estimates of max g for a given value of ρ than classical aggregates. We focus on two aggregation functionals within the class of induced aggregates which are closely related to the KS and p-norm functionals. The induced exponential functional is given by

$$c_{IE}(g, \rho) = \frac{\int_\Omega g\, e^{\rho g} d\Omega}{\int_\Omega e^{\rho g} d\Omega}. \tag{9}$$

Kennedy and Hicken (2015) show how c_{IE} can be obtained from c_{KS} by taking a Richardson extrapolation of c_{KS} to $\rho \to \infty$. The induced power functional is given by

$$c_{IP}(g, \rho) = \frac{\int_\Omega g^{\rho+1} d\Omega}{\int_\Omega g^{\rho} d\Omega}. \tag{10}$$

The induced power functional is only suited to strictly positive functions g (Kennedy and Hicken 2015). This is analogous to the p-norm functional requiring nonnegative g values to be effective.

The induced aggregation functionals also have discrete analogues for finite sets of constraints. The induced exponential function is given by

$$c_{DIE}(\rho) = \frac{\sum_{i=1}^{n_t} g_i e^{\rho g_i}}{\sum_{i=1}^{n_t} e^{\rho g_i}}. \tag{11}$$

The induced power function is given by

$$c_{DIP}(\rho) = \frac{\sum_{i=1}^{n_t} g_i^{\rho+1}}{\sum_{i=1}^{n_t} g_i^{\rho}}. \tag{12}$$

Similar to c_{IP}, c_{DIP} is only applicable if $g_i \geq 0$ for $i = 1, ..., n_t$. One advantage these induced aggregation functions possess over the classical aggregation functions is convergence to a single value for an arbitrary number of sample points. This is evident from the fact that functions (11) and (12) are ratios of sums rather than single sums.

3 Test problem

The test problem we will use to evaluate the different aggregation strategies is the structural optimization of the Common Research Model (CRM) wing. Originally, the CRM wing was developed as a test case for verifying the performance of computational fluid dynamics codes (Vassberg et al. 2008). Later, Kenway et al. (2014a) created a model structure for the wing as a test case for structural and aerostructural optimization methods. The layout of this wing structure is presented in Fig. 1. The size, geometry, and structure of the wing are based on those of a Boeing 777 civil transport aircraft.

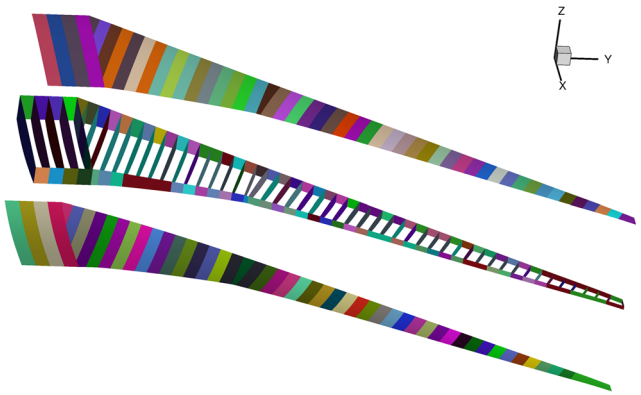

Fig. 1 Exploded view of wing structure. Skin thicknesses and stiffener properties are defined by design variables on each colored patch. Groups of colored patches define the domains for constraint aggregation

We briefly discuss the set of software tools used in our analysis. The coupled aerodynamic and structural properties of the wing at various flight conditions are analyzed using the MACH framework (MDO of aircraft configurations at high-fidelity) (Kenway and Martins 2014). The aerodynamic analysis was carried out using the SUMad CFD solver (van der Weide et al. 2006). SUMad is a multiblock, finite-volume solver for the Reynolds Averaged Navier-Stokes equations. Turbulent flow is computed using a one-equation Spalart–Allmaras model. Large deformations in the wing geometry were handled using a hybrid algebraic-linear elastic mesh warping scheme (Kenway et al. 2010). Changes in the wing geometry itself were computed using a free-form deformation volume approach (Kenway et al. 2010). The structural analysis was carried out by the toolkit for the analysis of composite structures (TACS) (Kennedy and Martins 2014a), a finite element solver specializing in thin-shell aerospace structures. The coupled aerodynamic and structural states were resolved using a nonlinear block Gauss–Seidel method with Aitken acceleration (Kenway et al. 2014b). The optimizer used in the framework is SNOPT (Gill et al. 2002), which is accessed through the pyOpt interface (Perez et al. 2012). This suite of tools may be used to carry out aerodynamic shape optimization (Lyu et al. 2014) and aerostructural optimization (Kenway et al. 2014a) but this work will focus only on structural optimization.

Our goal is to minimize the mass of the wing for a design aircraft subject to both yield stress and buckling constraints. We consider three symmetric load cases: a 2.5 g pull-up maneuver at sea level and 0.64 Mach number, a 1 g push-over maneuver at sea level and 0.64 Mach number, and a 1.95 g buffet load at 28 000 foot altitude and 0.85 Mach number. In order to accurately determine the loads for each load case, we perform a full aerostructural analysis to compute aerodynamic loads. The aircraft weight is assumed to be 297 550 kg in each case, regardless of changes in the wing mass.

The design variables of the problem are the skin panel thickness t_s, the stiffener height h_s, the stiffener thickness t_w, and the distance between stiffeners b, known as the pitch. The colored patches shown in Fig. 1 represent stiffened skin panels over which individual design variables apply. Figure 2 shows a cross-section of a typical skin panel and the definition of each variable. For simplicity, we let $t_b = t_w$ and $w_b = h_s$ in the stiffener model. In addition, a single variable defines the stiffener pitch on the entire lower skin, the entire upper skin, and both wing spars. Linear adjacency constraints are introduced for the thickness, stiffener thickness, and stiffener height variables to restrict the difference between the variable values in adjacent skin panels. In our finite element model, instead of modeling the stiffeners directly, the increase in stiffness resulting from the stiffeners is smeared over the whole panel. In total, the problem contains 842 design variables and 660 linear constraints.

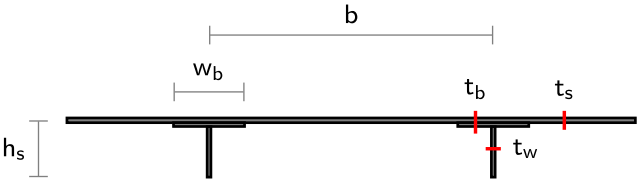

Fig. 2 Cross-section of a skin panel with the design parameters labelled. Only skin thickness t_s, stiffener height h_s, stiffener thickness t_w, and stiffener pitch b are independent variables in our problem

The failure criteria of the problem are aggregated over the four main wing components: lower skin, upper skin, spars, and ribs. Each component has one yield stress failure criterion and one buckling failure criterion per load case, for a total of 24 constraints. This number is reduced to 17 failure constraints by ignoring buckling for the wing skin that is in tension in each load case and ignoring yield stress failure for the 1.95 g buffet load case. The latter simplification is justified because those constraints are superseded by the yield stress failure in the 2.5 g load case. The number of constraints is altered by subdividing each component into more aggregation domains. We use between one and 40 domains per component, yielding between 17 and 680 failure constraints in the optimization problem.

4 Aggregation strategy comparison

In Section 2, we defined eight different functions that could be used for aggregating failure constraints in a structural optimization problem. In addition to selecting the aggregation function, the user must also select the aggregation parameter ρ and the number of domains into which the structure is split. As stated in the introduction, choosing larger parameter values and splitting the structure into more aggregation domains leads to a more accurate optimal mass estimate, but increases the cost of the optimization. Our goal with the remainder of this paper is to quantify the trade-off between accuracy and computational cost as we vary the aggregation scheme.

As stated in the Section 1, each aggregation scheme comprises a choice of aggregation function, a choice of aggregation parameter ρ, and a choice of how many domains into which each wing component is divided. Each component may be divided into one, two, five, ten, 20, or 40 smaller domains. For each choice of domains, we choose from among 13 possible values of the aggregation parameter between 20 and 500 and one of the eight aggregation functions described earlier. This yields a total of 624 possible aggregation schemes.

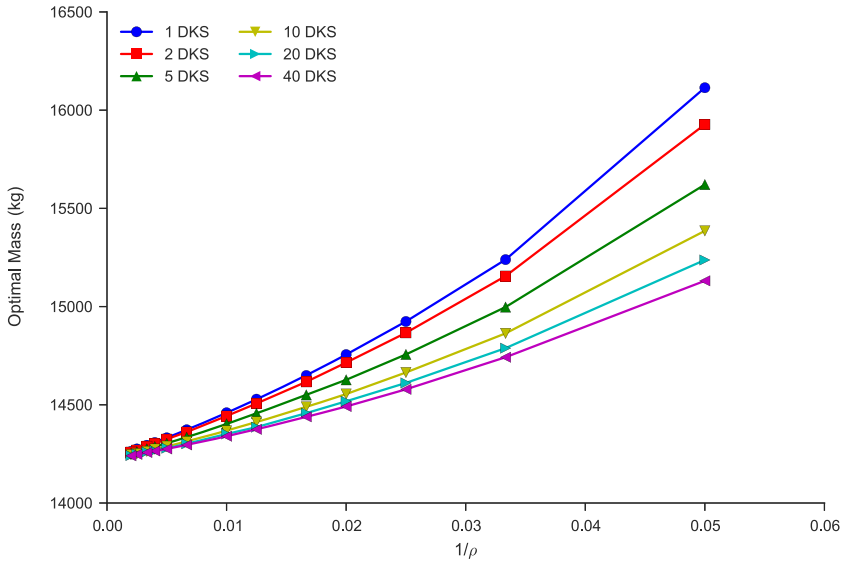

Fig. 3 Optimal mass spread using discrete KS aggregation. Increasing ρ and the number of constraints leads to more accurate optimal mass estimates

In each of the following sets of results, we set the optimality and feasibility parameters of SNOPT to 10^{-5} and use the "nonderivative linesearch" option. We set the maximum number of major and minor iterations so that they do not cause premature termination of the optimization solver. Otherwise, we use the default optimizer settings.

4.1 Discrete KS aggregation

Our first set of results was generated using the discrete KS function (DKS) given in (7). Figure 3 shows the optimal mass of the CRM structure for a range of different aggregation parameter values and number of aggregation domains. Figure 4 shows the same data, but focuses on the cases with a larger aggregation parameter. We plot our mass results in terms of the inverse of the aggregation parameter, $1/\rho$, to better show the convergence on a single "true" optimal mass value. (Recall that pushing $\rho \to \infty$ or $1/\rho \to 0$ results in a feasible domain that approaches that produced by using the maximum-value aggregation (1).) Using this knowledge and Fig. 4, we can estimate the true optimal mass of the structure to be around 14 220 kg.

Figures 3 and 4 clearly show the trade-off between the selection of the aggregation scheme and the accuracy of the optimum mass estimate. As expected, using more constraints (more aggregation domains) and a higher ρ value yields a more accurate optimal mass estimate. In the worst case of one aggregation domain per component, the optimum mass is overestimated by about 1890 kg (13.3 % of the optimal mass) for $\rho = 20$, 240 kg (1.68 %) for $\rho = 100$, and 40 kg (0.28 %) for $\rho = 500$. In the best case of 40 domains per component, the optimum mass is still overestimated by

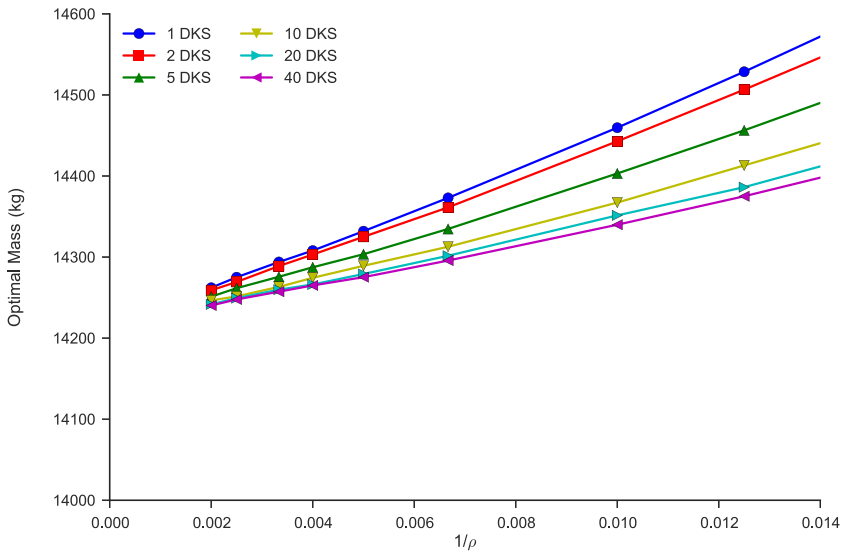

Fig. 4 Optimal mass spread using discrete KS aggregation and high ρ values. The optimal mass at $\rho = \infty$ appears to be 14 220 kg regardless of the number of constraints used

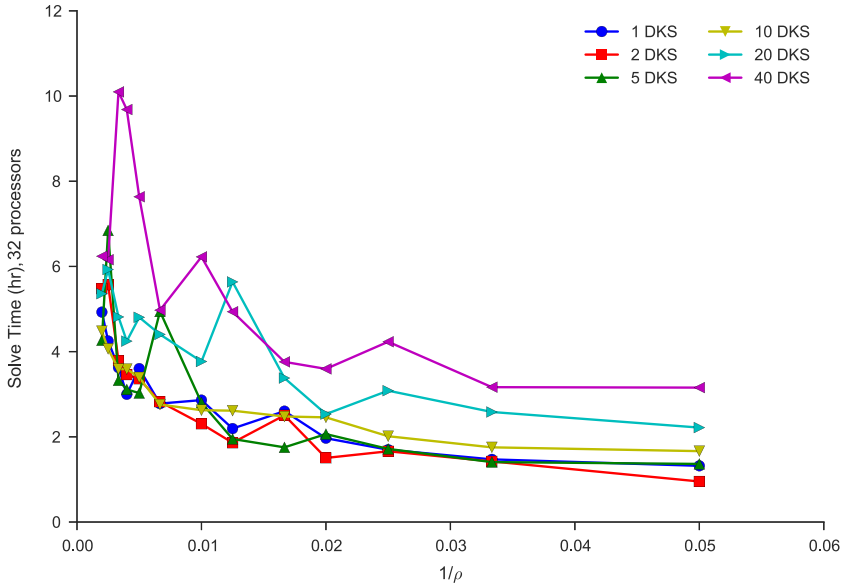

Fig. 5 Run time to determine the optimal mass using discrete KS aggregation. For less than ten aggregation domains per component, the run time is not sensitive to the number of constraints

890 kg (6.3 %) for $\rho = 20$, 120 kg (0.84 %) for $\rho = 100$, and 20 kg (0.14 %) for $\rho = 500$. Increasing ρ further for this problem would lead to an even narrower range of mass values but this level of accuracy may be unnecessary if other sources of error overwhelmed the error due to constraint aggregation.

Figures 3 and 4 show that increasing the number of constraints leads to a more accurate estimate of the optimum mass. However, the relative increase in accuracy diminishes with every increase in the number of constraints. Figure 4 shows that using ten aggregation domains per component (170 failure constraints) reduces the optimum mass by 75 % of the difference between one and 40 aggregation domains across all values of $\rho > 100$. In other words, we realize three-quarters of the accuracy improvement using one-quarter the number of constraints. If we are prepared to use half the maximum number of constraints, (340 constraints or 20 domains per component,) we realize 90 % of the benefit. Therefore, if ρ is large enough, the number of constraints need not be excessive to yield accurate estimates of optimum mass.

An issue that arises with increasing the number of constraints is the computational cost of the optimization. In particular, the cost of computing gradients at each iteration using the adjoint method scales with the number of constraints. Figure 5 shows the wall time of the optimization for each case presented in Fig. 3. As we expect, larger values of ρ lead to longer run times because of the increased curvature of the aggregated constraints and the resulting ill-conditioning in the optimization problem. For

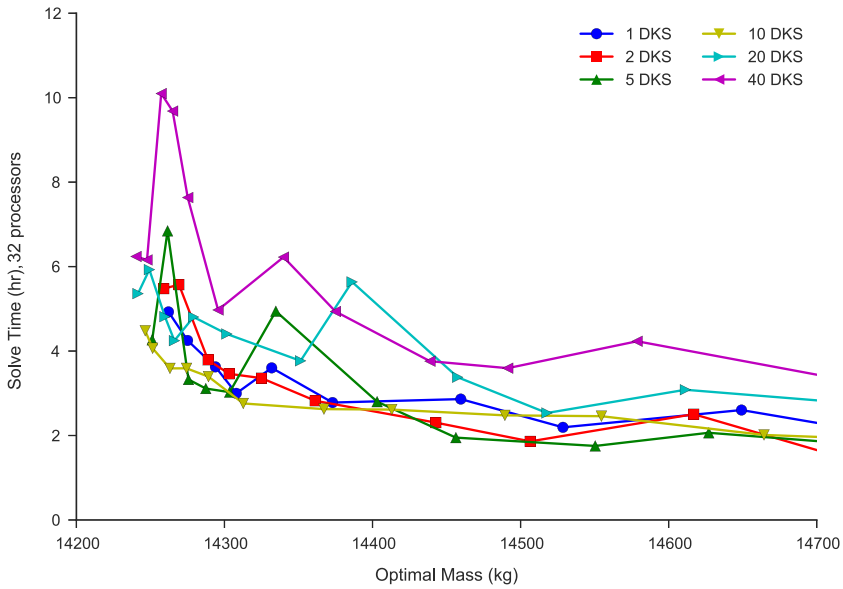

Fig. 6 Trade-off between run time and computed optimal mass using discrete KS aggregation. The aggregation scheme that provides the best balance between these objectives uses $\rho \approx 200$ and five to ten aggregation domains

$\rho \geq 200$, run time begins to rise rapidly. However, Fig. 5 also suggests that when the number of constraints is not too large (less than ten aggregation domains per component in our problem) the run time is insensitive to the number of constraints. The increased cost of evaluating more constraint gradients at each iteration is offset by a reduction in the number of iterations needed to solve the optimization problem.

The analysis of the solution data to this point suggests that there is a "sweet spot" or ideal trade-off between accuracy and computational effort. Figure 6 provides a visualization of that trade-off. It shows the same run time information as Fig. 5, but plotted against the optimal mass instead of ρ. Treating Fig. 6 as a solution plot for a multiobjective problem, we see that the ideal trade-off occurs using $\rho \approx 200$ and five to ten aggregation domains. If we are especially concerned about run time, we may choose a slightly lower value of ρ.

4.2 Continuous KS aggregation

We now compare the choice of aggregation function in addition to the choice of parameter and number of failure constraints. Our first comparison is between Equations (7) and (5), the discrete and continuous variants of KS aggregation. For clarity of presentation, we will only focus on the data for one, ten, and 40 aggregation domains per component. We have found that, when comparing the optimal mass of each case, the lines showing one and 40 domains always provide the upper and lower bounds of the solution. The lines for intermediate numbers of domains always appear arranged in their natural order between the lines for one and 40 domains. The ten-domain line represents our best estimate of the ideal trade-off between accuracy and computational cost.

Figure 7 compares the optimal mass values obtained from the continuous form (denoted KS) and discrete form (DKS) of KS aggregation. Using KS, the optimal mass is generally underestimated rather than overestimated. These contrasting behaviors in the limit of ρ can be explained by deriving the DKS aggregate in terms of the KS aggregate with a special choice of α.

$$\begin{aligned} c_{DKS} &= \frac{1}{\rho} \ln \left[\sum_i e^{\rho g_i} \right] \\ &\approx \frac{1}{\rho} \ln \left[\frac{n_t}{|\Omega|} \int e^{\rho g} \, d\Omega \right] \\ &= c_{KS}(\alpha = |\Omega|/n_t) \\ &= c_{KS}(\alpha = 1) + \frac{\ln(n_t/|\Omega|)}{\rho} \end{aligned}$$

In our tests, we have taken $\alpha = 1$, so c_{DKS} will always be larger than c_{KS} regardless of the choice of ρ and the number of domains. This leads to the counterintuitive result that a smaller number of failure constraints produces a more accurate estimate of the true optimal mass.

Figure 7 also confirms the result of Fig. 3 that only a fraction of the maximum number of failure constraints are needed to estimate the optimum mass resulting from using the maximum number of failure constraints. Overall, Fig. 7 shows that the optimal mass values computed using KS aggregation are more accurate than those using DKS aggregation. In the worst case of 40 aggregation domains, the optimal mass is underestimated by 670 kg (4.7 %) for $\rho = 20$, 200 kg (1.4 %) for $\rho = 100$, and 40 kg (0.28 %) for $\rho = 500$. In the case of one aggregation domain, the optimum mass is underestimated by -30 kg (-0.21 %) for $\rho = 20$, 90 kg (0.63 %) for $\rho = 100$, and 20 kg (0.14 %) for $\rho = 500$.

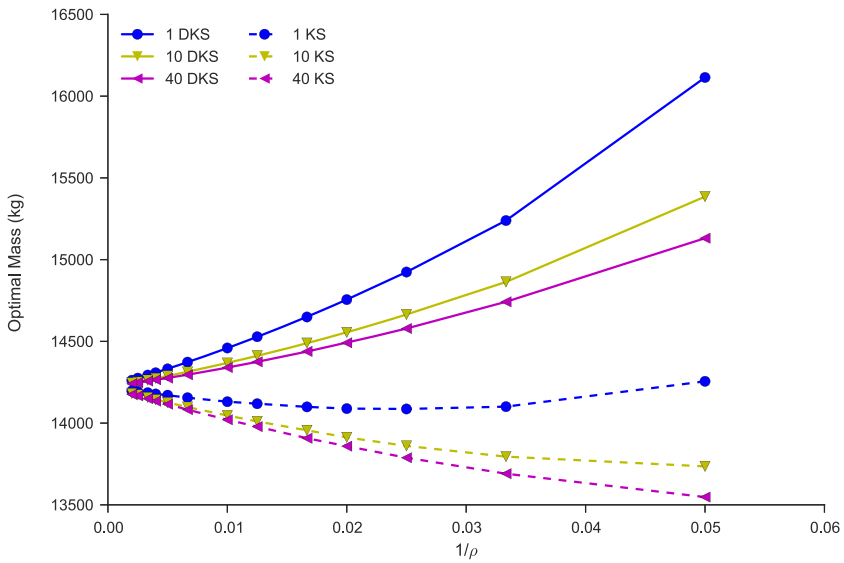

Fig. 7 Comparison of continuous and discrete KS aggregation. The continuous form of KS aggregation is not conservative, but produces more accurate estimates of the optimal mass

The nonmonotone behavior of the optimal mass for one domain in Fig. 7 raises the question of how the optimal design itself evolves as ρ increases. Figures 8 and 9 plot the differences with the $\rho = 500$ case for two sets of design variables: the stiffener height and the stiffener thickness. As we might expect, the differences between the $\rho = 500$ case and $\rho = 100$ case are smaller than those between the $\rho = 500$ and $\rho = 20$ case. However, while the optimum stiffener thickness increases with increasing ρ over much of the wing—indicated by the positive difference value in Fig. 9—the optimum stiffener height decreases with increasing ρ. These two trends have competing influences on the optimal mass; the higher thickness increases optimal mass while the lower height decreases optimal mass. Therefore, the nonmonotone behavior can be explained by a rapid decrease in stiffener height as ρ increases for a small number of aggregation domains. When more domains are used, as shown in Fig. 10, the difference in optimal height is lower and the difference in optimal thickness is greater, mitigating the nonmonotone change in optimal mass with ρ.

The run time for obtaining the optimal masses using the KS aggregation is plotted in Fig. 11. These run times can be directly compared with those obtained using DKS aggregation. Clearly, the run times obtained using both types of aggregation functions are similar regardless of the number of failure constraints. In terms of the cost-accuracy trade-off, the results in Figs. 7 and 11 argue in favor of using KS

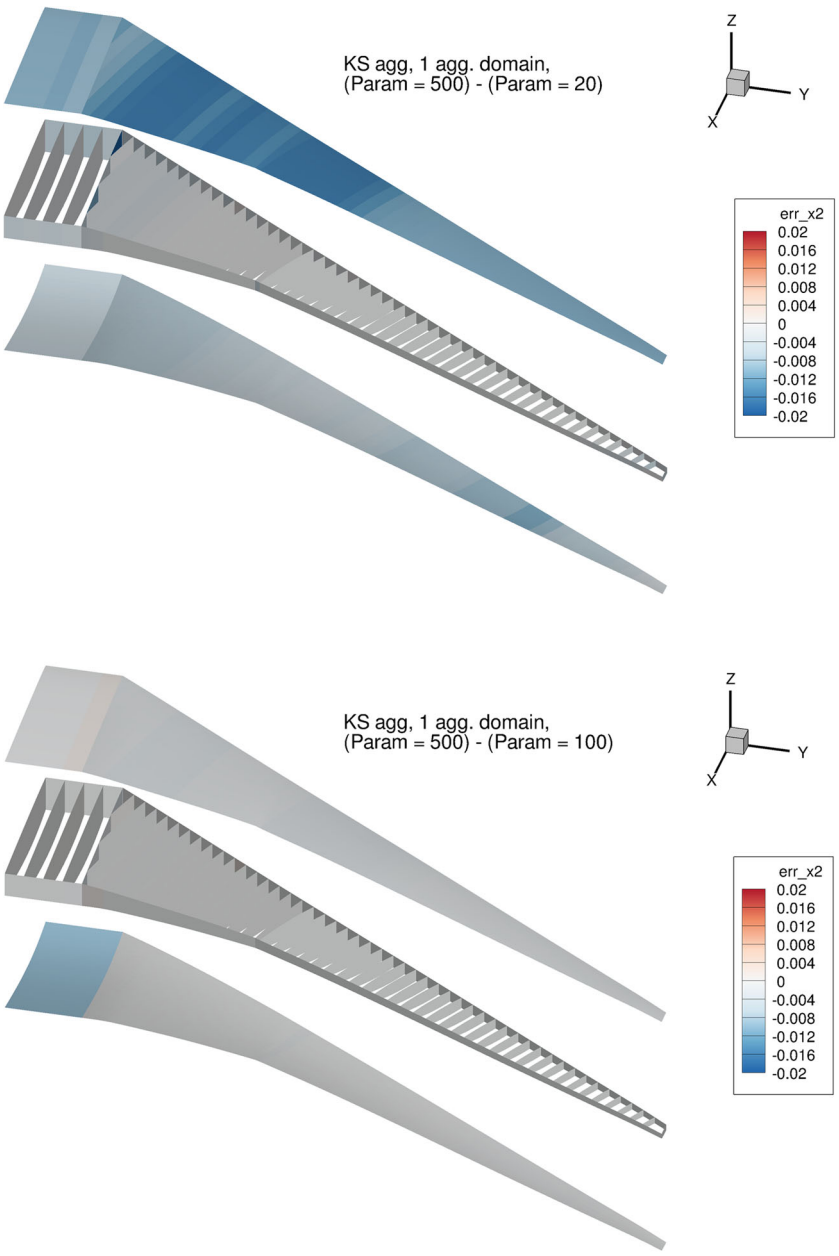

Fig. 8 Difference in optimal panel stiffener height between $\rho = 500$ and $\rho = 20$ (*top*) and between $\rho = 500$ and $\rho = 100$ (*bottom*) using KS aggregation over one domain per component. The stiffeners are taller for a smaller value of ρ

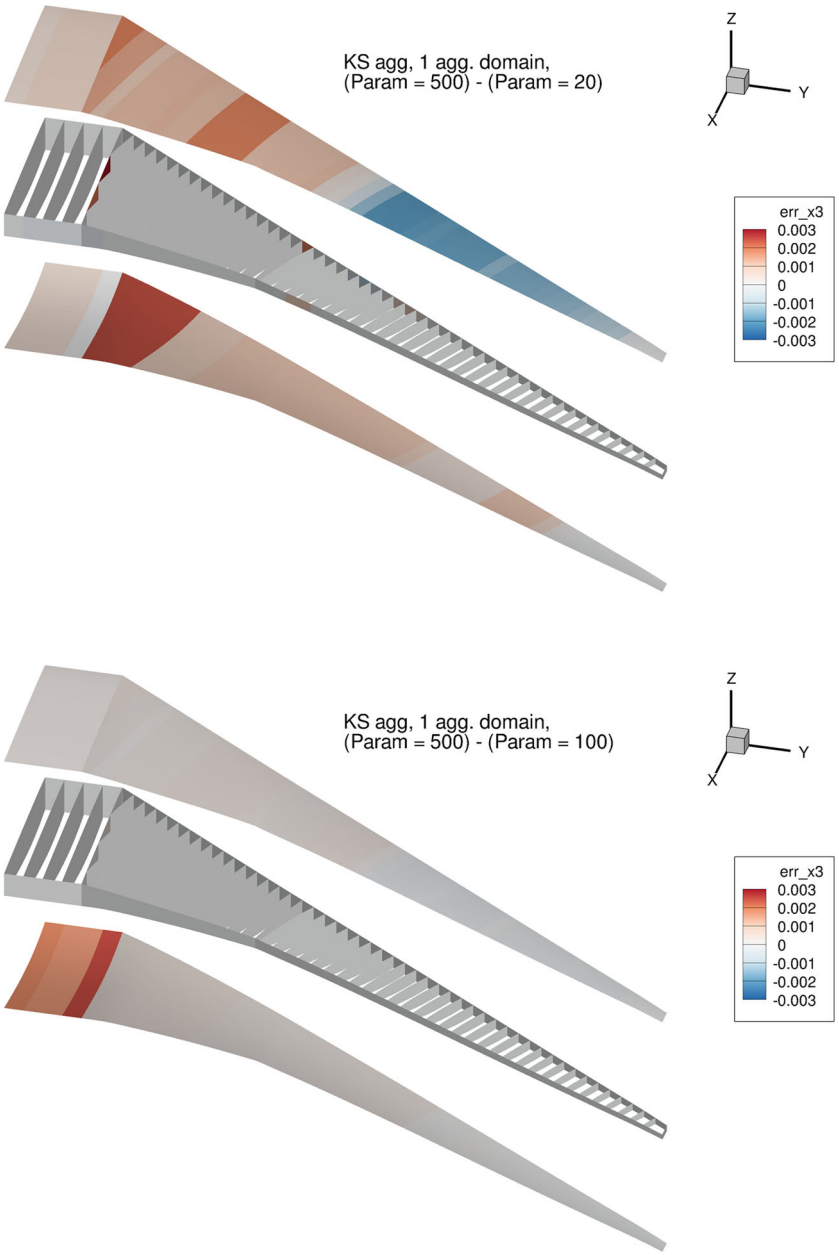

Fig. 9 Difference in optimal panel stiffener thickness between $\rho = 500$ and $\rho = 20$ (*top*) and between $\rho = 500$ and $\rho = 100$ (*bottom*) using KS aggregation over one domain per component. The stiffeners are thinner for a smaller value of ρ. Coupling this result with Fig. 8, a small ρ value causes the stiffeners to be tall and thin while a larger ρ value causes the stiffeners to be shorter and thicker

aggregation in place of DKS aggregation because a more accurate solution can be obtained in a similar computational time.

4.3 *p*-norm aggregation

As mentioned in Section 2, both the discrete form (8) and the continuous form (6) of p-norm aggregation are only appropriate for failure functions that evaluate to nonnegative values. The buckling constraints in this problem do not fit that criterion. Tensile loads cause the buckling criterion to become negative and the absolute value of that negative number can cause a large overestimation of the buckling criterion in the aggregate. Nevertheless, we attempted to use these aggregation schemes in the optimization problems to see how much progress SNOPT could make from the starting point. In every case, SNOPT terminated after only a few minor iterations with the error that it could not satisfy the nonlinear constraints. We interpret this to mean that the negative values in the buckling criterion caused so much overestimation of the aggregated buckling failure that the problem became infeasible. We do not consider the discrete or continuous p-norm aggregation strategies further in this study.

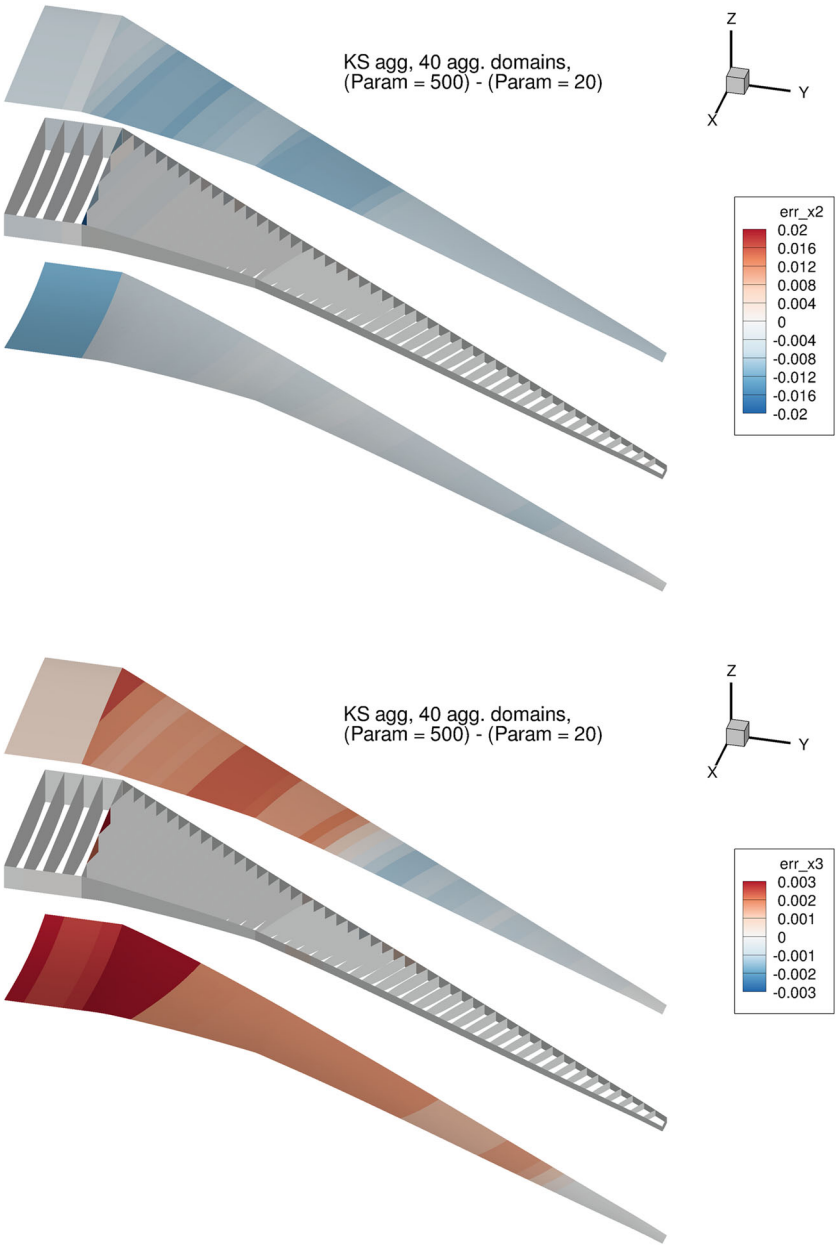

Fig. 10 Difference in optimal panel stiffener height (*top*) and thickness (*bottom*) between $\rho = 500$ and $\rho = 20$ using KS aggregation and 40 domains per component. The difference in optimal height is smaller, compared to Fig. 8, and the difference in optimal thickness is larger, compared to Fig. 9, mitigating the nonmonotone behaviour of the optimal mass with changing ρ

4.4 Induced exponential aggregation

We now directly compare KS aggregation with its induced counterpart, induced exponential aggregation. Figure 12 compares the optimal masses obtained using the continuous form of induced exponential aggregation (IE) (9) with those obtained using KS aggregation. Like KS aggregation, we observe that, counterintuitively, using more IE-aggregated failure constraints reduces the accuracy of the optimal mass estimate. In addition, using more constraints has the advantage of producing a more predictable progression of the optimal mass as ρ increases. The most interesting feature of Fig. 12 is that each optimal mass curve for IE aggregation resembles a reflected version of the corresponding KS aggregation curve. IE aggregation overestimates the optimal mass where KS aggregation underestimates it, and vice-versa.

The main advantage of IE aggregation in place of KS aggregation is the rapid decrease in the spread of optimal mass values with increasing ρ. Figure 13 shows the same data as Fig. 12, but focuses on the results for the largest values of ρ. The optimal mass spread—the difference between the optimal masses of the one domain and 40 domain tests—for $\rho = 100$ is about 30 kg or 0.21 % of the optimal mass. For $\rho = 500$, the spread is about 5kg or 0.035 % of the optimal wing mass. By comparison, the same spread values using KS aggregation are 110 kg (0.77 %) and 20 kg (0.14 %) respectively. By using IE aggregation in place of

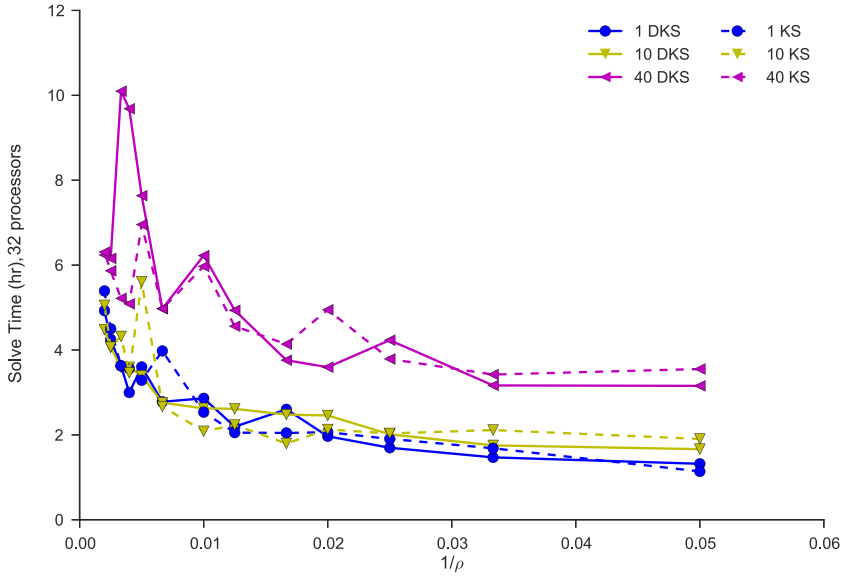

Fig. 11 Run time comparison between KS and DKS aggregation schemes. Both strategies yield similar run times for the same parameter values and number of domains

KS, the spread has been reduced by 70–75 % for large values of ρ. Using IE aggregation with one domain per component, the most accurate in terms of optimal mass, the mass is overestimated by 40 kg (0.28 %) for $\rho = 100$ and 10 kg (0.070 %) for $\rho = 500$. Adding the spread in the optimal mass to the error in the best case, we see that for $\rho \geq 100$ and any number of failure constraints, the maximum error in the optimal mass is about 1.4 % using KS aggregation but only 0.5 % using IE aggregation. Therefore, using IE aggregation in place of KS aggregation reduces the error in the optimal mass estimate by more than 60 %.

There is a computational price to be paid for this level of accuracy. Figure 14 plots the run time required to solve the optimization problems for each case displayed in Figs. 12 and 13. Regardless of the choice of ρ and the number of constraints used, the problems that used IE aggregation required much more computational effort. Both aggregation methods used the same quadrature scheme to evaluate the failure constraints, so this increase in effort must be caused by the difficulty of solving the optimization problem, i.e., the number of major iterations taken by SNOPT. This result suggests that robust optimization algorithms are needed in order to use IE aggregation reliably.

Figures 15 and 16 compare the optimal masses obtained between the continuous and discrete (DIE) (11) forms of induced exponential aggregation. For small values of ρ and a small number of aggregation domains, there is a significant difference between the optimal mass values. Furthermore, the spread in optimal mass is much higher using DIE aggregation than using IE aggregation. However, as both ρ and the number of aggregation domains increases, the difference in optimal mass decreases rapidly. For $\rho \geq 100$,

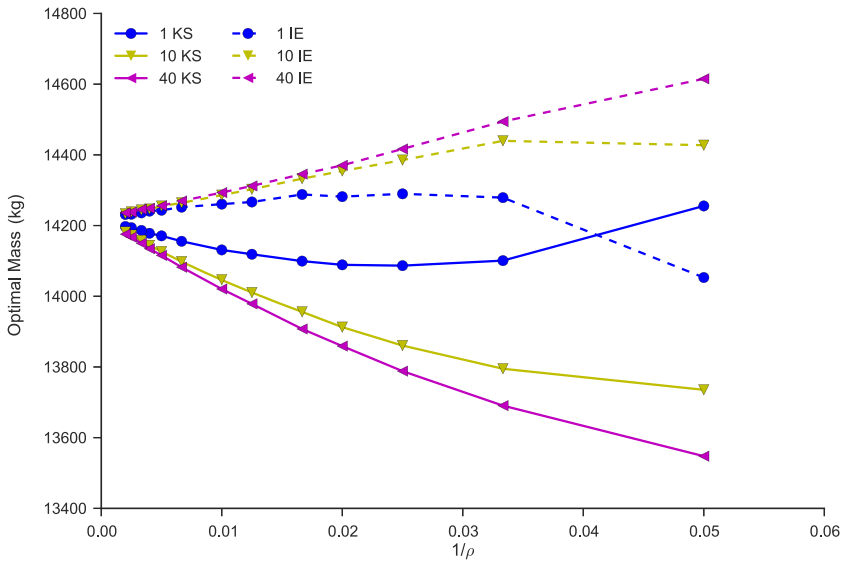

Fig. 12 Optimal mass comparison of KS and IE aggregation. Using IE aggregation results in a more accurate estimate of the optimal mass regardless of the number of constraints and the choice of ρ

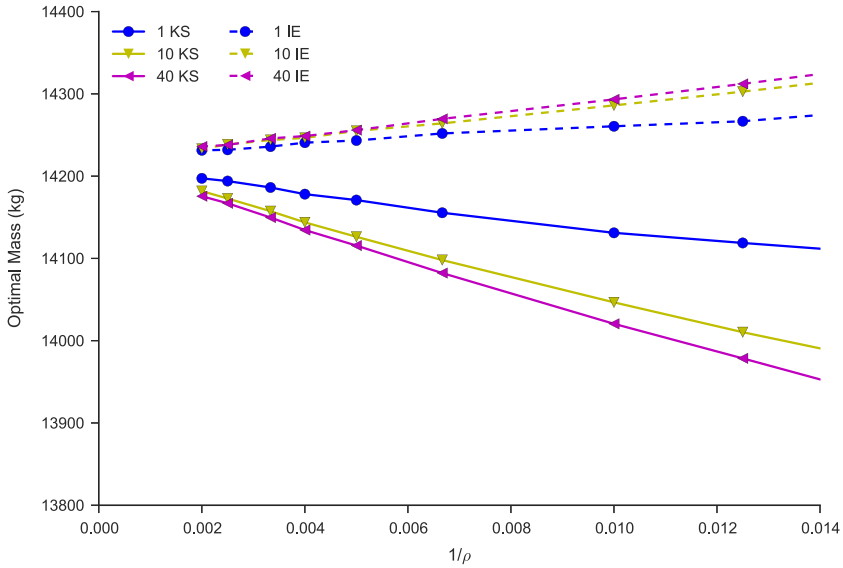

Fig. 13 Optimal mass comparison of KS and IE aggregation emphasizing high ρ values. The spread in optimal mass values using IE aggregation with different numbers of constraints rapidly decays with increasing ρ

both the continuous and discrete forms yield nearly identical results.

Figure 17 compares the run times of IE and DIE. While there is significant noise in the data, (most likely due to variations in the optimal search path,) neither aggregation method reliably computes the optimal solution in less time than the other. Our recommendation, therefore, is to use the continuous form of IE aggregation over the discrete form because of the smaller spread in the optimal mass value discussed above.

4.5 Induced power aggregation

In principle, the continuous (IP) (10) and discrete (DIP) (12) forms of induced power aggregation should suffer from the same deficiency as p-norm aggregation. That is, they cannot be used for failure criteria that evaluate to negative values. In practice, however, SNOPT had no difficulty satisfying the induced power constraints. We were able to obtain converged results for all selected values of ρ and all choices of the number of aggregation domains. This result is due to the absence of the absolute value operator in the IP and DIP aggregates. Using the p-norm aggregates, the absolute value operator caused large tensile loads to infect the aggregated buckling failure criteria and the optimization problem became infeasible. In IP and DIP aggregation, the negative values are preserved in the aggregate because either ρ or $\rho + 1$ leads to an odd power for a positive integer ρ. Therefore, for integer values of ρ, using IP and DIP does not destroy the feasibility of the optimization problem.

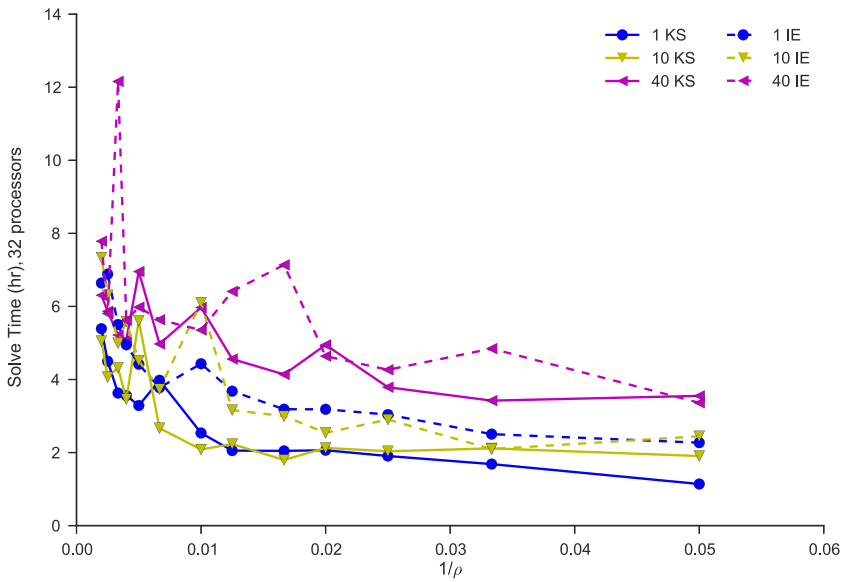

Fig. 14 Run time comparison of KS and IE aggregation. Optimizing with IE aggregation is more computationally expensive across all values of ρ and any number of constraints

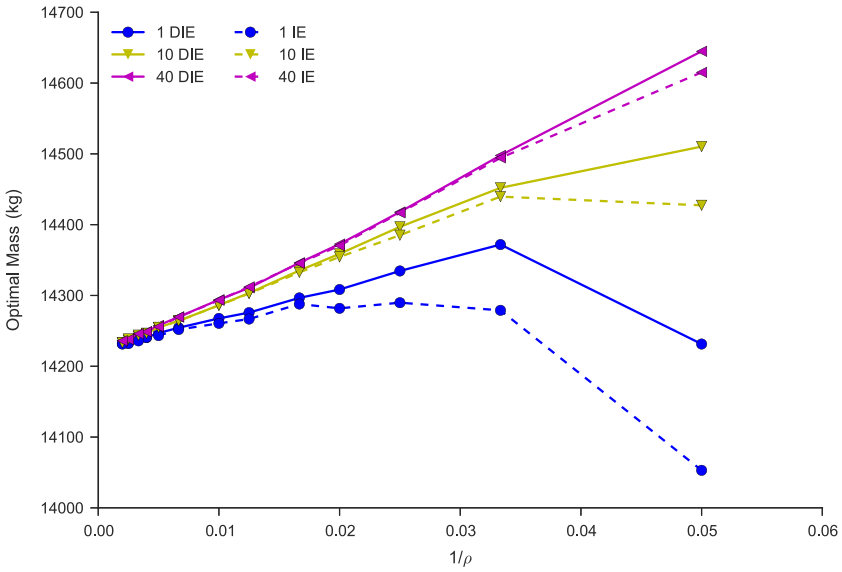

Fig. 15 Optimal mass comparison between IE and DIE aggregation. The discrete and continuous forms of IE aggregation produce similar optimal masses for large values of ρ

Figure 18 compares the optimal masses obtained using IE and IP aggregation. While the optimization processes converge successfully using IP aggregation, the optimal mass does not converge to the same value when a smaller number of aggregation domains are used. If more domains are used and ρ is sufficiently large, IP aggregation produces optimal masses that are virtually identical to those produced using IE aggregation. If the failure criteria for the problem always returned nonnegative values, we conjecture that both aggregation methods would produce the same result.

Figure 19 shows the major difference between the optimal designs computed with IE and IP aggregation for one domain per wing component. The figure shows the difference in stiffener pitch (the spacing between stiffeners) between the two optimal solutions for the largest ρ value. Using IP aggregation, the optimal design has the stiffeners placed farther apart on the ribs and therefore reduces their number and the mass of the whole wing box as a result. Figure 20 shows the impact this change has on the buckling criterion for the 2.5 g load case. Even though both designs are feasible with respect to their respective constraints, the design from IP aggregation shows higher buckling loads, both positive and negative, on its ribs.

The presence of both positive and negative values of the buckling criterion on the wing ribs in Fig. 20 explains why IE and IP aggregation yield optimal designs that differ only on the wing ribs. On both skins and the wing spars, the stresses are either all tensile or all compressive so the aggregation of these stresses will necessarily be tensile or compressive. On the ribs, however, there is a mixture of tensile and compressive stresses. Integrating the failure criterion over the domain causes these stresses to cancel each

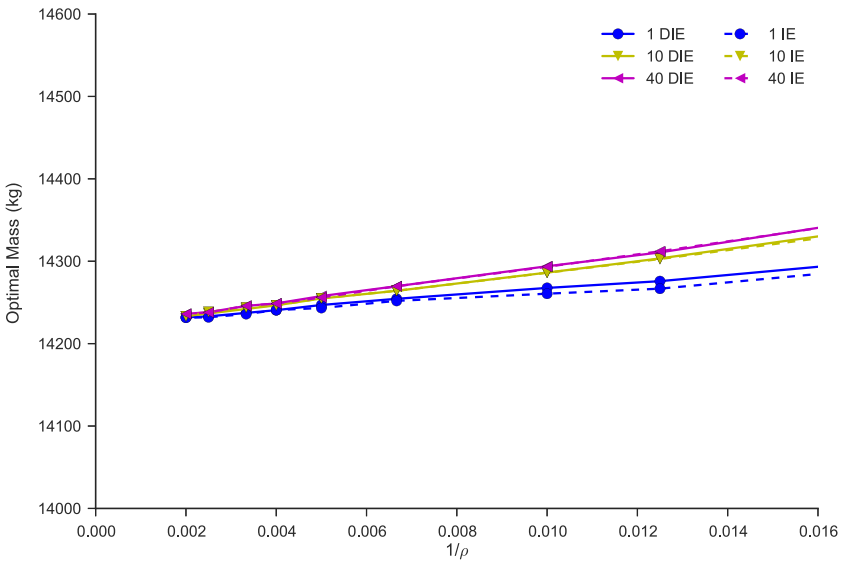

Fig. 16 Optimal mass comparison between IE and DIE aggregation focusing on large values of ρ. For $\rho \geq 100$, the two aggregation functions produce virtually identical results

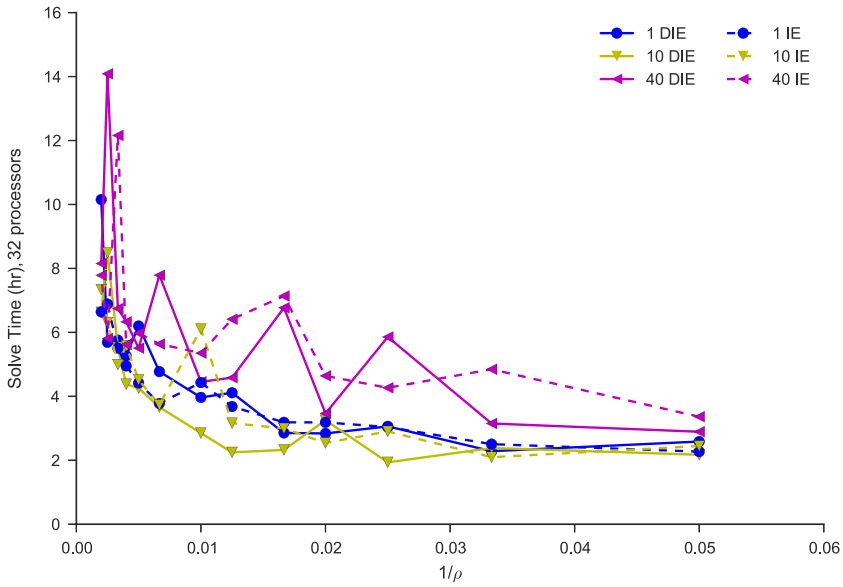

Fig. 17 Run time comparison of IE and DIE aggregation. Neither aggregation scheme has a clear advantage in terms of computational effort

other out in the aggregate. This effect can result in a local violation of the buckling constraint that is not picked up by the aggregate, regardless of the quadrature scheme used to evaluate the integral. Figure 21 clearly shows this local violation of the buckling constraints. Note that this cancellation phenomenon cannot occur in IE aggregation because the exponential term prevents it. As the number of aggregation domains increases, there is less opportunity for mixed loading to occur in a given aggregation domain, and the optimal designs from IP and IE aggregation move into agreement. While this analysis demonstrates that IP aggregation is more robust than p-norm aggregation, in that it is less likely to lead to an infeasible problem, it is still not as robust as IE aggregation in its handling of negative values of failure criteria.

Figure 22 compares the run times for IE and IP aggregation. Generally, the run times using the two different aggregation strategies are similar. The main exception is the case of one aggregation domain and large values of ρ. However, we attribute this behavior to the difficulty of handling the mixed loading in the ribs using IP aggregation. Using more domains mitigates these ill effects and produces run times similar to those found with IE aggregation.

As with IE and DIE aggregation, the differences in the results observed between IP and DIP aggregation are minute when large values of ρ and many aggregation domains are used. Figure 23 compares the optimal mass values while Fig. 24 compares run time. Because the error in the optimal mass is smaller for the same computational effort, we recommend using IP aggregation in place of DIP aggregation

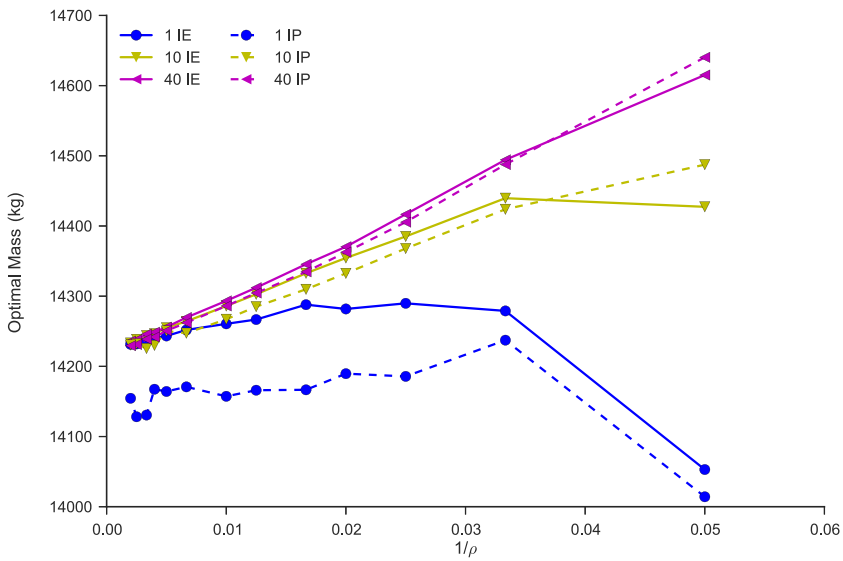

Fig. 18 Optimal mass comparison between IE and IP aggregation. Both aggregation methods produce similar results if many constraints are present

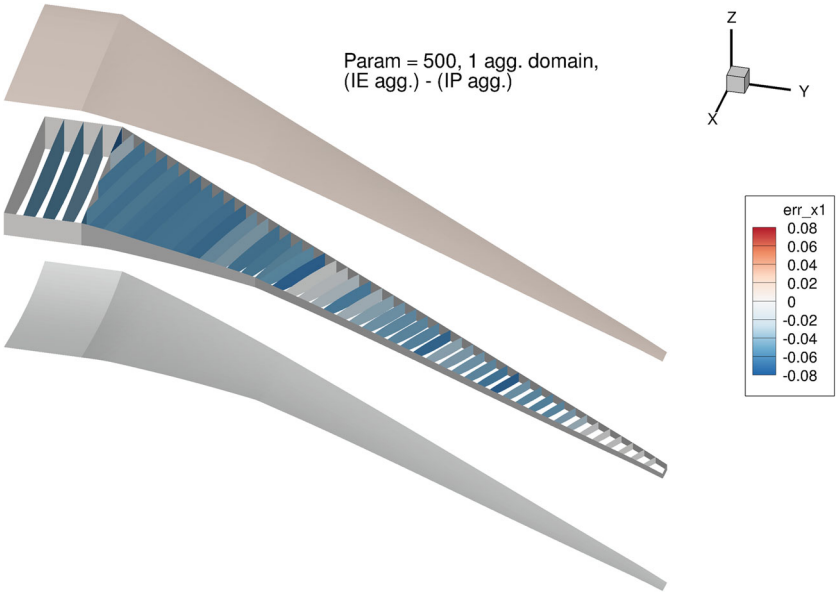

Fig. 19 Difference in stiffener pitch between the optimal designs obtained using IE and IP aggregation with $\rho = 500$ and one aggregation domain per component. Optimization with IP aggregation produces higher pitch values on most of the ribs

in general, if the problem allows. However, the similarity in the solutions between IE and IP aggregation suggests that IE is the preferred aggregation method in terms of optimal solution accuracy.

4.6 Mesh refinement study

Another important factor in estimating the optimal mass in structural design is the finite element mesh itself. For consistency in the results, the aggregation function should converge to a single value as the element size is reduced to zero for a fixed design. Of the functions tested in this study, only the discrete KS and p-norm aggregation methods do not have this property, due to their sensitivity to the number of trial points (Kennedy and Hicken 2015). As the element size decreases, changes in the stress field may lead to different optimal designs. In the next series of tests, we aim to study the mesh dependence of the optimal solution.

In the mesh refinement tests, we use IE aggregation with $\rho = 100$ and ten domains per component. We optimize the wing design using both second-order and third-order plate elements. From our baseline mesh, we size the average element so that each refinement contains about 10 000 more elements than the next-coarsest mesh. We created five different meshes of between 10 000 and 50 000 elements and optimized the wing design on all of them. Note that these changes to the mesh do not change either the number of variables or the number of constraints in the optimization problem.

Figure 25 plots the optimal mass results for our mesh refinement study. Figure 26 plots the corresponding run times. While both the second-order and third-order meshes do converge on similar optimal mass values, using a second-order mesh with this aggregation strategy appears to yield a more accurate estimate of the true optimal mass for a coarse mesh, despite the lower run time. This result may be analogous to the result, seen in Fig. 12, that using fewer domains with IE aggregation yields a more accurate estimate of the optimum mass. In comparison with the mass errors due to the aggregation scheme, the mass error due to using a coarse mesh is much higher. The data in Fig. 25 do not point to

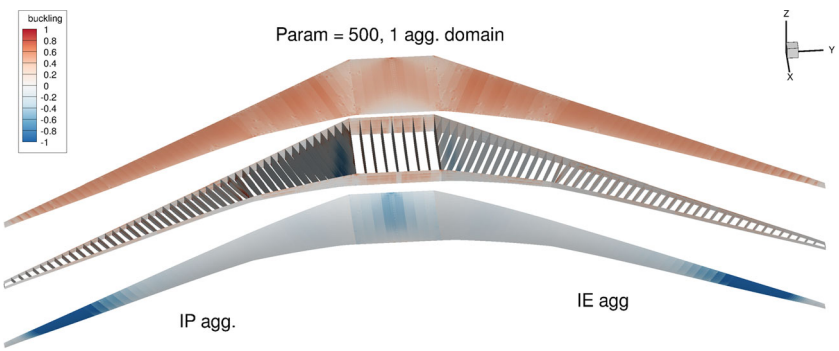

Fig. 20 Comparison of buckling criterion values between optimal designs obtained using IE and IP aggregation with $\rho = 500$ and one aggregation domain per component. The ribs are the only part of the wing structure where we observe a mixture of tensile and compressive loads

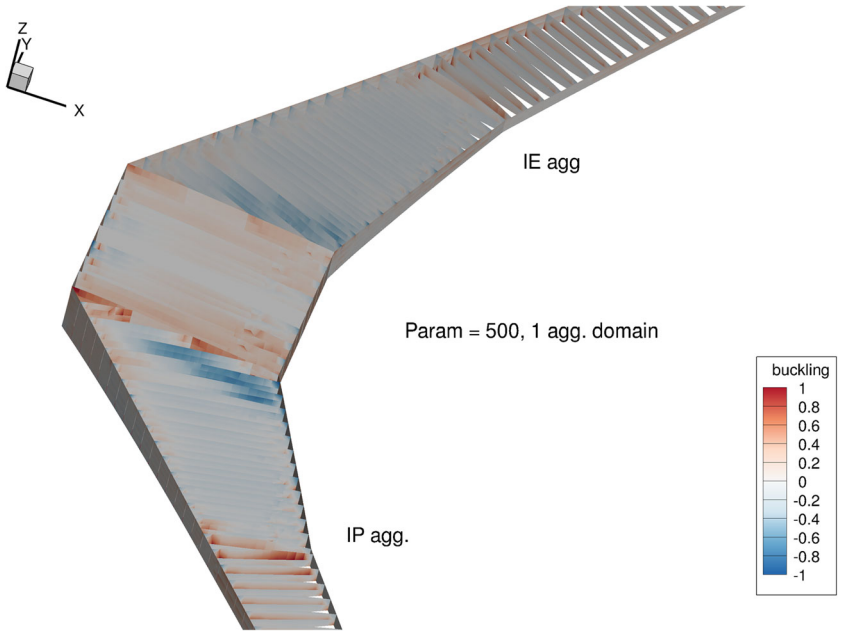

Fig. 21 Same data as Fig. 20, but focused on the ribs. The high positive values of the buckling criterion observed on some ribs of the IP optimum are infeasible with respect to the IE constraints. In the aggregation, however, they are offset by the high negative values observed on ribs near the wing root

a clear estimate of the true optimal mass, but the optimal mass computed by the second order mesh falls in a 600-kg range of values. The optimal mass computed by the third order mesh falls in a 1400-kg range of values. By comparison, the range of mass values displayed in Fig. 12 for every IE aggregation scheme is less than 500 kg. If we only consider $\rho \geq 100$, the range of mass values is less than 100 kg. These results all suggest that the choice of mesh can be even more important than the choice of constraint aggregation method for obtaining an accurate optimal mass estimate in stress-constrained structural optimization.

5 Discussion and recommendations

Our study is fundamentally limited to one large structural optimization problem. Because of the smeared stiffness model employed in the structural analysis, multiple variables on each panel could be used to increase the apparent stiffness of that panel. We found that this resulted in multiple local minima on this optimization problem when only yield stress failure was constrained. Therefore, we are not able to compare the KS and p-norm aggregation directly or to compare p-norm with IP aggregation directly. We could

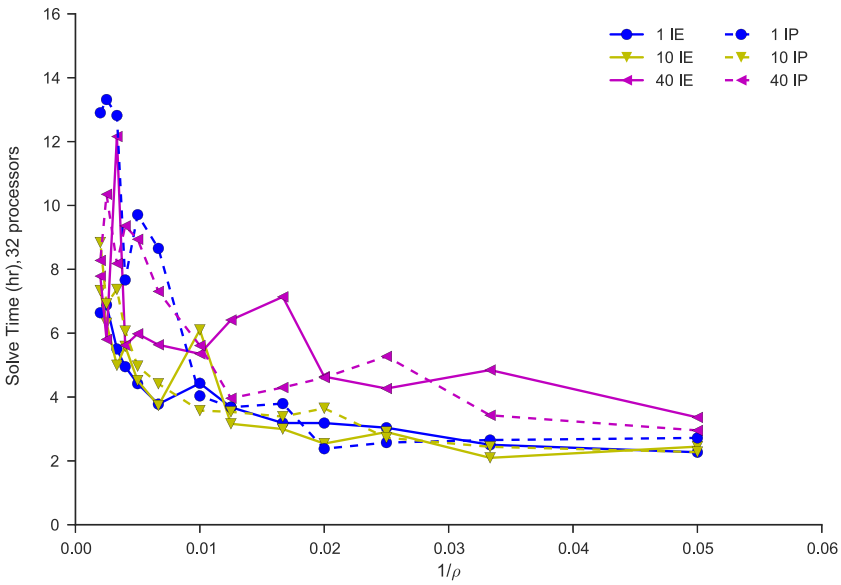

Fig. 22 Run time comparison between IE and IP aggregation. Except for cases where IP aggregation fails to find the correct optimum, both aggregation strategies require similar computational time

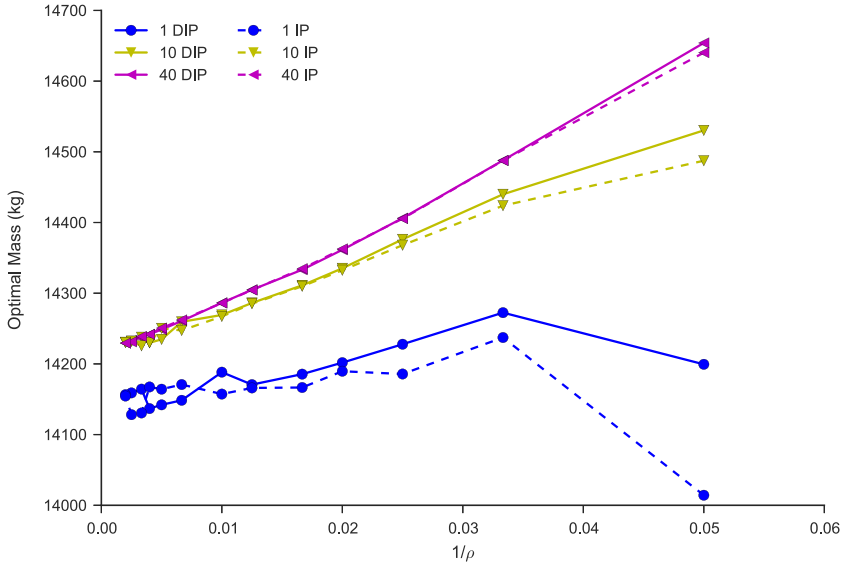

Fig. 23 Optimal mass comparison between IP and DIP aggregation. As with IE and DIE, differences between the optimal mass values disappear either by using more constraints or by using a larger value of ρ

mix the aggregation types in a single problem, such as using KS functions for the buckling failure and p-norm functions for the yield stress failure, but have not done so to better study the aggregation methods themselves.

With the above limitation in mind, we present some general recommendations for employing constraint aggregation based on our results.

Continuous vs. discrete aggregation While some discrete aggregation methods are conservative with respect to failure at prescribed points in the domain, they also exhibit mesh-dependence and produce less accurate estimates of the true optimum mass compared to their continuous analogues. These properties are especially evident when a small value of ρ is chosen. Because conservatism is so difficult to enforce on a domain of finite size, and because they showed better performance in our tests, we recommend employing the continuous form of the aggregation in general problems.

Classical vs. induced aggregation In terms of computational cost, regardless of the number of constraints in the problem, induced aggregation methods require longer run times than the corresponding classical aggregation methods. In terms of both solution accuracy and the range of applicable problems, the induced aggregation methods are clearly superior. Therefore, we recommend their use if high accuracy in the optimal design is required.

Number of aggregation domains Using more aggregation domains generally leads to an optimization problem

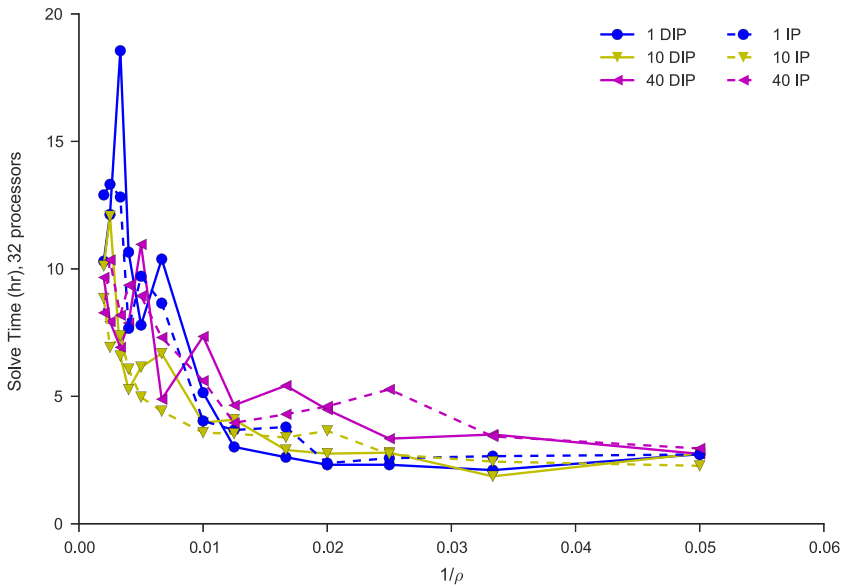

Fig. 24 Run time comparison between IP and DIP aggregation. As with IE and DIE, there is no clear advantage of either strategy

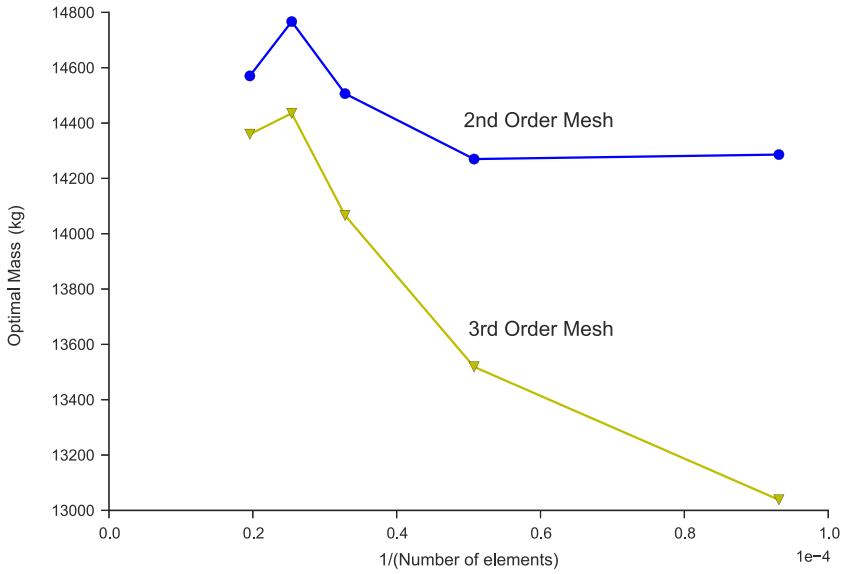

Fig. 25 Optimal mass comparison between using second and third-order finite element meshes. Both meshes seem to produce converging optimal mass as the number of elements increases. However, the range of optimal mass values is much higher than the range obtained when comparing constraint aggregation strategies

that can be solved in fewer iterations, reducing computational effort. However, increasing the number of constraints increases the number of gradients to be computed at each iteration, increasing computational effort. As noted in the literature (París et al. 2010; Le et al. 2010), using a modest number of aggregation domains instead of a large number can greatly reduce computational cost while providing an accurate optimal design. Our study reconfirms this practice. However, in our test problem, we found that the two competing factors driving computational cost were well-balanced. For a specific choice of aggregation function and parameter, using up to ten aggregation domains per component — 40 domains in total, or 170 constraints over three load cases — did not substantially change the run time from using one domain per component. In other words, we found no computational drawback to increasing the number of constraints up to a threshold of 40 aggregation domains. We emphasize that this result strongly depends on the software employed. The TACS software (Kennedy and Martins 2014a) can efficiently evaluate many gradients using a combination of the adjoint method and a direct solver for the linear system. Using less-efficient techniques to evaluate the gradients, such as finite differences, would favour using fewer aggregation domains to mitigate cost.

Selection of aggregation parameter The aggregation parameter must be selected to balance the accuracy of the feasible domain with the ill-conditioning produced by the precise estimate of sharp corners in the domain. Several references in the literature (Wrenn 1989; Raspanti et al. 2000;

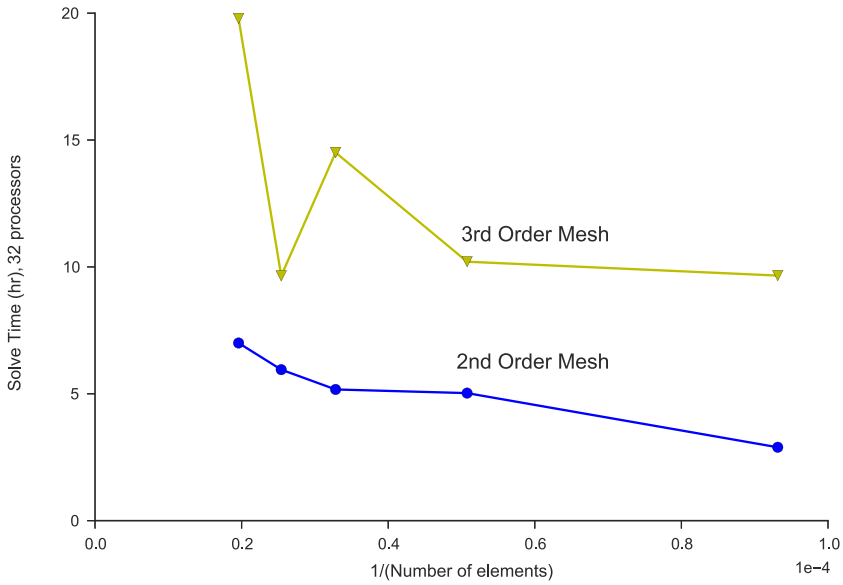

Fig. 26 Run time comparison between second and third-order finite element meshes. Not surprisingly, using a lower-order mesh greatly reduces computational effort

Akgün et al. 2001; Poon and Martins 2007) suggest a value of $\rho = 50$ to balance these considerations. However, our results using SNOPT indicate that the computational time does not rapidly increase with increasing ρ until values greater than 100 are used. Therefore, if a robust optimization algorithm is used, we recommend using $\rho = 100$ or even larger values in general problems.

6 Conclusions

In this work, we applied a range of aggregation strategies to a structural mass minimization problem subject to failure constraints. Our problem considered the design of a wing box under three load conditions for which both yield and buckling failure constraints were enforced. We provided empirical data to quantify the trade-off between the accuracy of the solution obtained using aggregated failure constraints and the computational cost of obtaining the optimal solution.

We found that using up to 40 domains over which to aggregate failure criteria on our test structure did not substantially impact wall time to obtain the optimal solution with efficient adjoint sensitivity calculations. To increase the accuracy of the optimal mass estimate, we recommend using the induced exponential aggregation strategy in place of the KS or p-norm strategies now commonly in use. We also recommend setting the aggregation parameter ρ to 100 to balance accuracy of the optimal solution and ill-conditioning of the optimization problem. Taken together, these recommendations yielded an optimal structural design that had a mass of within 0.5 % of the true optimal design. We found that this error was well below the error introduced by using a coarse or low-order finite element mesh. The influence of the mesh on the optimal design was not considered in depth and remains open to investigation.

Acknowledgments The authors would like to thank Gaetan K. W. Kenway for his assistance in setting up the CRM wing geometry used in this paper. Computations were performed on the GPC supercomputer at the SciNet HPC Consortium. SciNet is funded by: the Canada Foundation for Innovation under the auspices of Compute Canada; the Government of Ontario; and the University of Toronto.

References

Akgün MA, Haftka RT, Wu KC, Walsh JL, Garcelon JH (2001) Efficient Structural Optimization for Multiple Load Cases Using Adjoint Sensitivities. AIAA J 39(3):511–516. doi:10.2514/2.1336

Duysinx P, Bendsøe MP (1998) Topology optimization of continuum structures with local stress constraints. Int J Numer Methods Eng 43:1453–1478

Duysinx P, Sigmund O (1998) New developments in handling stress constraints in optimal material distribution. In: Proceedings of the 7th AIAA/USAF/NASA/ISSMO Symposium on Multidisciplinary Analysis and Optimization, vol 1

Gill PE, Murray W, Saunders MA (2002) SNOPT: An SQP algorithm for large-scale constrained optimization. SIAM J Optim 12(4):979–1006

Holmberg E, Torstenfelt B, Klarbring A (2013) Stress constrained topology optimization. Struct Multidiscip Optim 48:33–47. doi:10.1007/s00158-012-0880-7

Kennedy GJ (2015) Strategies for adaptive optimization with aggregation constraints using interior-point methods. Comput Struct 153:217–229. doi:10.1016/j.compstruc.2015.02.024

Kennedy GJ, Hicken JE (2015) Improved constraint-aggregation methods. Comput Methods Appl Mech Eng 289:332–354. doi:10.1016/j.cma.2015.02.017

Kennedy GJ, Martins JRRA (2014a) A parallel finite-element framework for large-scale gradient-based design optimization of high-performance structures. Finite Elements in Analysis and Design 87:56–73. doi:10.1016/j.finel.2014.04.011

Kennedy GJ, Martins JRRA (2014b) A parallel aerostructural optimization framework for aircraft design studies. Struct Multidiscip Optim 50(6):1079–1101. doi:10.1007/s00158-014-1108-9

Kenway GKW, Martins JRRA (2014) Multipoint high-fidelity aerostructural optimization of a transport aircraft configuration. J Aircr 51(1):144–160. doi:10.2514/1.C032150

Kenway GKW, Kennedy GJ, Martins JRRA (2010) A CAD-Free Approach to High-Fidelity Aerostructural Optimization. In: 13th AIAA/ISSMO Multidisciplinary Analysis and Optimization Conference, Fort Worth,TX. doi:10.2514/6.2010-9231

Kenway GKW, Kennedy GJ, Martins JRRA (2014a) Aerostructural optimization of the Common Research Model configuration. In: 15th AIAA/ISSMO Multidisciplinary Analysis and Optimization Conference, Atlanta. doi:10.2514/6.2014-3274

Kenway GKW, Kennedy GJ, Martins JRRA (2014b) Scalable parallel approach for high-fidelity steady-state aeroelastic analysis and adjoint derivative computations. AIAA J 52(5):935–951. doi:10.2514/1.J052255

Kreisselmeier G, Steinhauser R (1979) Systematic Control Design by Optimizing a Vector Performance Indicator. In: Symposium on Computer-Aided Design of Control Systems, IFAC, Zurich, Switzerland, pp 113-117

Kreisselmeier G, Steinhauser R (1983) Application of Vector Performance Optimization to a Robust Control Loop Design for a Fighter Aircraft. Int J Control 37(2):251–284. doi:10.1080/00207179.1983.9753066

Lambe AB, Martins JRRA (2016) Matrix-free aerostructural optimization of aircraft wings. Struct Multidiscip Optim 53(3):589–603

Le C, Norato J, Bruns T, Ha C, Tortorelli D (2010) Stress-based topology optimization for continua. Structural and Multidisciplinary Optimization 41(4):605–620. doi:10.1007/s00158-009-0440-y

Lyu Z, Kenway GKW, Martins JRRA (2014) Aerodynamic Shape Optimization Investigations of the Common Research Model Wing Benchmark. AIAA J 53(4):968–985. doi:10.2514/6.2014-0567

París J, Navarrina F, Colominas I, Casteleiro M (2009) Topology optimization of continuum structures with local and global stress constraints. Struct Multidiscip Optim 39:419–437. doi:10.1007/s00158-008-0336-2

París J, Navarrina F, Colominas I, Casteleiro M (2010) Block aggregation of stress constraints in topology optimization of structures. Adv Eng Softw 41:433–441. doi:10.1016/j.advengsoft.2009.03.006

Perez RE, Jansen PW, Martins JRRA (2012) pyOpt: A Python-Based Object-Oriented Framework for Nonlinear Constrained Optimization. Struct Multidiscip Optim 45(1):101–118. doi:10.1007/s00158-011-0666-3

Poon NMK, Martins JRRA (2007) An adaptive approach to constraint aggregation using adjoint sensitivity analysis. Struct Multidiscip Optim 34:61–73. doi:10.1007/s00158-006-0061-7

Qiu GY, Li XS (2010) A note on the derivation of global stress constraints. Struct Multidiscip Optim 40:625–628. doi:10.1007/s00158-009-0397-x

Raspanti CG, Bandoni JA, Biegler LT (2000) New strategies for flexibility analysis and design under uncertainty. Comput Chem Eng 24:2193–2209. doi:10.1016/S0098-1354(00)00591-3

Vassberg JC, DeHaan MA, Rivers SM, Wahls RA (2008) Development of a Common Research Model for applied CFD validation studies. AIAA:2008–6919

van der Weide E, Kalitzin G, Schluter J, Alonso J (2006) Unsteady Turbomachinery Computations Using Massively Parallel Platforms. In: 44th AIAA Aerospace Sciences Meeting and Exhibit, Aerospace Sciences Meetings, American Institute of Aeronautics and Astronautics. doi:10.2514/6.2006-421

Wrenn GA (1989) An Indirect Method for Numerical Optimization Using the Kreisselmeier–Steinhauser Function. Tech. rep. NASA Langley Research Center, Hampton, VA